ACS Biomaterials SCIENCE & ENGINEERING

pubs.acs.org/journal/abseba

Article

Patterning Neuroepithelial Cell Sheet *via* a Sustained Chemical Gradient Generated by Localized Passive Diffusion Devices

Ningwei Li,[▽] Feiyu Yang,[▽] Subiksha Parthasarathy, Sarah St. Pierre, Kelly Hong, Narciso Pavon, ChangHui Pak, and Yubing Sun*

Cite This: https://doi.org/10.1021/acsbiomaterials.0c01365

Read Online

ACCESS | Metrics & More | Article Recommendations | Supporting Information

ABSTRACT: Recent advances in human pluripotent stem cells (hPSCs)-derived *in vitro* models open a new avenue for studying early stage human development. While current approaches leverage the self-organizing capability of hPSCs, it remains unclear whether extrinsic morphogen gradients are sufficient to pattern neuroectoderm tissues *in vitro*. While microfluidics or hydrogel-based approaches to generate chemical gradients are well-established, these systems either require continuous pumping or encapsulating cells in gels, making it difficult for adaptation in standard biology laboratories and downstream analysis. In this work, we report a new device design that leverages localized passive diffusion, or LPaD for short, to generate a stable chemical gradient in an open environment. As LPaD is operated simply by media changing, common issues for microfluidic systems such as leakage, bubble formation, and contamination can be avoided. The device contains a slit carved in a film filled with solid gelatin and connected to a static aqueous morphogen reservoir. Concentration gradients generated by the device were visualized *via* DAPI fluorescent intensity and were found to be stable for up to 168 h. Using this device, we successfully induced cellular response of Madin−Darby canine kidney (MDCK) cells to the concentration gradient of a small-molecule drug, cytochalasin D. Furthermore, we efficiently patterned the dorsal−ventral axis of hPSC-derived forebrain neuroepithelial cells with the sonic hedgehog (Shh) signal gradient generated by the LPaD devices. Together, LPaD devices are powerful tools to control the local chemical microenvironment for engineering organotypic structures *in vitro*.

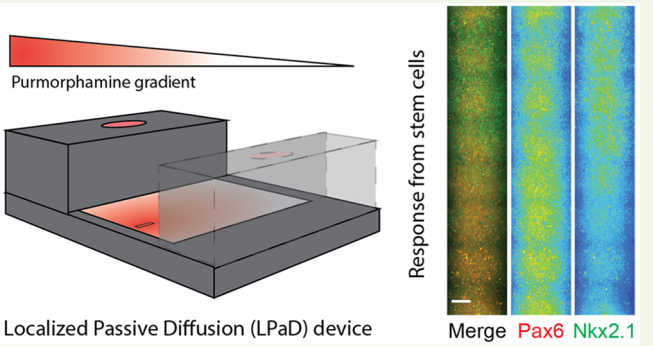

KEYWORDS: *human pluripotent stem cells, neuroepithelium, chemical gradient, microfluidics, patterning*

INTRODUCTION

Recent findings suggest that human brains develop quite differently from rodent brains,[1,2] and the accessibility of neurulation-stage human embryos is limited by practical and ethical reasons.[3] Thus, there is a growing interest in developing *in vitro* models for early stage neural development based on human pluripotent stem cells (hPSCs). Brain organoids that are derived by culturing hPSCs in 3D matrixes mimic the structure of various brain regions.[4,5] However, as the derivation of brain organoids relies on the spontaneous differentiation of hPSCs, they are often irreproducible and heterogeneous in cytoarchitecture.[6,7] Due to the challenge in delivering desirable small molecules or growth factors to specific regions in 3D spheroids, it is difficult to establish precise arealization and axial patterning. More recently, we and others pioneered a new strategy to generate neuroectoderm models *in vitro* using 2D micropatterned culture systems.[8−11] While these approaches can generate neural rosettes or concentric rings of neuroepithelial cells, neural crest cells, and epidermal cells, a fully patterned neuroepithelium with proper anterior−posterior (A−P) and/or dorsal−ventral (D−V) axes has not been achieved.

In vivo, the D−V patterning of the neural tube is dictated by the concentration gradients of sonic hedgehog (Shh) secreted by the notochord and floor plate and BMP and Wnt family proteins, which are produced dorsally by epidermis.[12] Producing morphogenic concentration gradients *in vitro* to pattern tissues is a feasible and biomimetic approach to fabricate patterned neuroepithelium. There are two primary strategies to generate concentration gradients for cell culture. The first strategy utilizes microfluidic perfusion channels to control the flow rate and thus generate a concentration gradient due to restricted diffusion.[13−15] This approach can precisely generate a regionalized gradient as cell culture

Received: September 14, 2020
Accepted: March 12, 2021

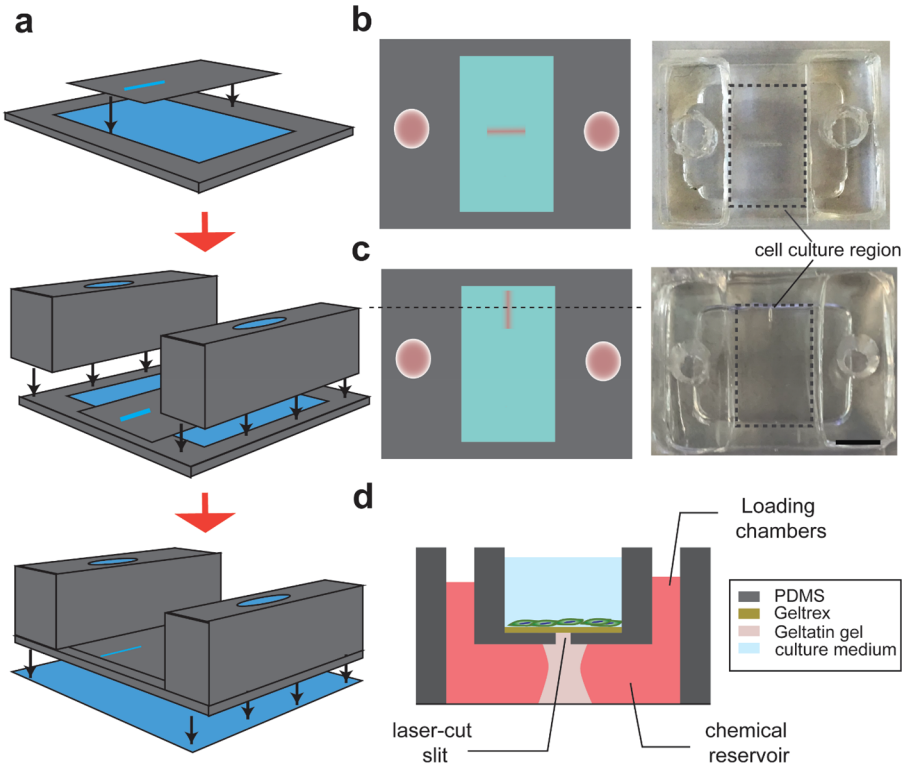

Figure 1. Fabrication process of the LPaD device. (a) Device fabrication procedure. (b) Top view schematic (left) and photo (right) of a device used for calibrating gradient stability. (c) Top view schematic (left) and photo (right) of a device used for establishing a gradient in the anterior−posterior axis. Scale bar, 5 mm. (d) Side view schematic of the gradient generating device showing where cells are grown; blue, cell culture media without additional chemical; pink, cell culture media with chemicals added.

chambers are predesigned and properly located within the generated concentration gradient. However, the microfluidic system requires pumps to continuously provide the required molecules and media to maintain the concentration gradient. Thus, subtle defects can drastically change the fluidic dynamics and disrupt the pattern of the concentration gradient. In addition, for long-term cell culture, the cost of maintaining a continuous flow of expensive growth factors or morphogens is immense, making it impractical to use this approach for protracted culturing. The second strategy uses source-sink diffusion across a hydrogel barrier, taking advantage of the porosity of hydrogels.[16] While a sustained gradient can be generated without continuously pumping, the cells need to be encapsulated in the hydrogels to sense the gradient. Thus, this method is not feasible for patterning 2D cell sheets. Moreover, the gradients generated by such passive diffusion devices are difficult to control and span a relatively large 3D space, making it difficult to precisely pattern millimeter-sized microtissues. The diffusive profile relies on the material properties of hydrogels, which may also affect stem cell differentiation. Instead of using hydrogels, passive diffusion microfluidic devices have also been developed for studying cell communications,[17] cell migration,[18] and drug delivery.[19] The diffusion can be driven by concentration difference,[20] surface tension,[21] and gravity.[22] However, a cleanroom environment is usually needed for fabricating those devices, making them less accessible for many laboratories. Recently, it has been demonstrated that an extrinsic gradient of Shh can induce dorsal−ventral neural patterning in microfluidic devices[23] and 3D organoids using Shh expressing cells.[24] These important works show great promise to fully control neural tissue patterning. However, these approaches either require a complicated microfluidic device with cells embedded in hydrogels or require genetically modified hPSCs lines that may not be accessible for many researchers. Therefore, a simpler, easy-to-use approach is still needed for a broader application of this concept.

In this work, we present a new device design that can establish a stable concentration gradient. We term this device as LPaD as it generates the concentration gradient through Localized Passive Diffusion. The entire device can be autoclaved for sterilization and placed in a 6-well plate format for cell culture and requires minimum preparation and maintenance, which is ideal for long-term stem cell culturing and differentiation. We observed that the gradient generated from our device was stabilized by the 12th hour from the addition of small-molecule chemicals and could be maintained for up to 168 h. In MDCK cells, we validated that actin depolymerization could be controlled by a small-molecule inhibitor cytochalasin D (CytoD) in a gradient manner. In hPSC-derived neuroepithelium, we achieved successful patterning of the D−V axis using a Shh agonist purmorphamine. These results validate the utility of this device design in multiple cellular applications and provide a novel and easy-to-use platform for studying patterning synthetic embryonic tissues *in vitro*.

METHODS

Device Fabrication. The frame of a LPaD device was made with polydimethylsiloxane (PDMS), and the designs are illustrated in Figure 1a. Dow Corning Sylgard 184 silicone elastomer base and curing agent (GMID: 04019862) were first mixed in a 10:1 ratio. Next, 30 g (10 g) of un-cross-linked PDMS was poured into 100 mm

https://doi.org/10.1021/acsbiomaterials.0c01365
ACS Biomater. Sci. Eng. XXXX, XXX, XXX−XXX

Petri dishes and subsequently baked at 65 °C for at least 2 h until it solidified into 5 mm (2 mm) thick slabs (10 mm × 20 mm), respectively. The thick slab was cut into the loading inlet and outlet, while the thin slab was cut to make the chemical chamber (step 1, Figure 1a). A thin slit (200 μm in width on average) at various lengths was cut onto a 1/32 in. PDMS film by a laser cutter (40 W Epilog Mini 18 × 12) at 20% speed, 80% power, 2500 Hz frequency, and 600 DPI resolution with vector job type to form a slit. The cut PDMS film was then glued with PDMS to the chemical chamber, and the inlet and outlet were glued to the side of the PDMS film (step 2, Figure 1a). Gaps between the inlet/outlet and the PDMS film were sealed with PDMS. Coverslips (Φ = 25 mm) were plasma cleaned (PDC-001, Harrick plasma) and bound to the bottom of the chemical chamber by PDMS (step 3, Figure 1a). For calibration experiments without cells, 1/32 in. silicone films (Ean: 0604339345964) was used instead of PDMS films. The dimensions of each part are illustrated in Figure S1.

It is notable that PDMS can absorb hydrophobic small molecules,[25] which may affect the stability of the chemical gradient in the long term. To address this issue, PDMS can be coated with molecules such as parylene to prevent absorption.[26] Alternatively, the LPaD device can be fabricated using acrylics, which is a nonporous material and compatible with a laser cutter (Figure S2).

MDCK Cell Culture. Madin−Darby canine kidney (MDCK) cells were cultured in a T-25 flask with culture media, consisting of 87% DMEM (11960051, Gibco, ThermoFisher), 10% FBS (10082147, Gibco, ThermoFisher), 1 × MEM NEAA (11140050, Gibco, ThermoFisher), 1 × GlutaMAX (35050061, Gibco, ThermoFisher), and 1 × penicillin−streptomycin (15140122, Gibco, ThermoFisher). MDCK cells were subconfluent passaged at a 1:10 ratio at a seeding density of 10 000/cm^2 every 4−5 days. To detach the cells, cells were washed with 1 × DPBS and incubated at 37 °C with 3 mL of 0.25% Trypsin-EDTA (25200072, Gibco, ThermoFisher) for 3 min. The cell suspension was then mixed with 5 mL of culture media and centrifuged for 5 min at 1200 rpm. The supernatant was aspirated, and the cells were resuspended with 1 mL of culture medium. The cells can be seeded on the LPaD device for experiments.

Before cell seeding, the LPaD devices were sterilized by autoclaving. Gelatin (12.5%, G1890-100G, Sigma-Aldrich) solution and 25 mg/mL transglutaminase (Moo Glue, transglutaminase TI formula) solution were made and filtered with 0.22 μm filters to sterilize. To create cross-linked gelatin, the gelatin solution and transglutaminase solution were mixed in a 4:1 ratio, and 20 μL of the mixture was pipetted into the slit on the PDMS film until the slit was filled with gel. The gel created a diffusion channel that linked the chamber and the cell culture region. As cell attachment to the cross-linked gelatin was limited, only a small volume of the gel was used to fill the slit without occupying the cell culture region. The LPaD devices were placed in 6-well plates, incubated at 37 °C overnight, and then baked at 65 °C for 30 min to deactivate all unreacted enzymes. Next, the cell culture region was coated with 400 μL of 5 μg/mL fibronectin (33016015, Invitrogen) by incubating for 1 h at room temperature. The cell suspension (0.4 mL) was added to the cell culture region of the device with a cell seeding density of 50 000/cm^2. The device with the cells was incubated at 37 °C overnight. After cell attachment, culture media was aspirated, and 3 mL of fresh culture media was added to each well. Next, the cells were exposed to the cytochalasin D (CytoD) gradient for 24 h by adding 2.5 μM CytoD (PHZ1063, Gibco, ThermoFisher) to the chemical chamber.

hPSC Cell Culture and Differentiation. hPSCs (WAe009-A, WiCell, H9) were maintained in the 60 mm tissue culture dish coated with Geltrex (A1413202, Gibco, ThermoFisher) using E8 medium (A1517001, Gibco, ThermoFisher). The dishes were coated with 1% Greltrex in DMEM-F12 (11320033, Gibco, ThermoFisher) for 1 h at 37 °C and 1 h at room temperature. hPSCs were rinsed with 1 × DPBS, then incubated with 3 mL of 0.5 mM EDTA (15575038, Invitrogen) for 5 min at 37 °C. The EDTA was then aspirated, and hPSCs were removed from the dish by gently pipetting the cells with 4 mL of prewarmed E8 medium using a 5 mL serological pipet. Cells (400−600 μL) were seeded, and the cells were passaged every 4−5 days.

Similar to MDCK cell seeding, the LPaD devices were filled with a cross-linked gelatin solution. Geltrex (0.4 mL, 3.33%) in DMEM-F12 was pipetted onto the PDMS film to cover the entire cell culture area and incubated for 1 h at 37 °C and 1 h at room temperature. E8 medium with 10 μM ROCK inhibitors (Y27632, 10005583, Cayman Chemical) was prepared and left at room temperature until reaching equilibrium. hPSCs were rinsed with 1 × DPBS and incubated with 3 mL of 0.5 mM EDTA for 5 min at 37 °C. After aspirating the EDTA solution, a 1 mL pipet was used to flush stem cells off the tissue culture plates using 1 mL of the E8 medium with 10 μM ROCK inhibitors.

To culture hPSCs in the LPaD device, an appropriate amount of the cell suspension was first added to the cell culture area of the LPaD device, so that each device has 0.4 mL of cell suspension with a cell seeding density of 75 000 cells/cm^2. Devices with cells were incubated at 37 °C overnight. Seeding media were then aspirated, and 3 mL of E8 media was added to each well. Cells were cultured in E8 media for another 24 h before differentiation. To induce the differentiation of hPSCs into neuroepithelial cells with forebrain identities, the E8 media were changed to E6 media (A1516401, Gibco, ThermoFisher) supplemented with 0.1 μM LDN-193189 (19396, Cayman Chemical), 10 μM SB-431542(13031, Cayman Chemical), and 5 μM XAV939 (13596, Cayman Chemical). Three milliliters of the differentiation media was added to each well. To induce the Shh chemical gradient, 0.3 mL of 100 μM purmorphamine (a Shh agonist, 10009634, Cayman Chemical) solution prepared using the same differentiation media was added to the chemical chamber.[27] Differentiation media and purmorphamine solutions were changed every day until day 6 since the start of the differentiation. This differentiation protocol was adopted from the recent work by Cederquist et al.[24]

Immunocytochemistry. The cells were fixed with 4% PFA prepared in 1 × DPBS at room temperature for 20 min after the differentiation process was completed. The cells were then gently washed with 1 × DPBS three times until no PFA was left. Triton X-100 (0.1%, BP151500, Fisher BioReagents) was added to permeabilize the cell membranes for 30 min at room temperature, and then, the samples were washed three times with 1 × DPBS. The cell culturing area (the PDMS film) was cut from the device at this point. For MDCK cells, the cells were incubated in 1 × phalloidin (A12379, Life Technologies) and 15 μM 4,6-diamidino-2-phenylindole (DAPI, D1306, Invitrogen) at room temperature for 1 h. For hPSCs, cells were first incubated in 10% goat serum (16210072, Gibco, ThermoFisher) for 3 h at room temperature. Then, the cells were incubated in primary antibodies (see Table 1 in the Supporting Information) diluted in 10% goat serum (50 μL per sample) overnight at 4 °C and stained using corresponding secondary antibodies and counterstained using DAPI.

Simulation. *Estimation of Small-Molecule Diffusivity.* On the basis of the molecular structure, DAPI's radius of gyration was estimated as half of the length of three benzene rings at 0.4 nm. Using the Stokes−Einstein equation, at 37 °C, the diffusivity of DAPI in water can be calculated as

$$D = \frac{k_b T}{6\pi\eta a} = 8 \times 10^{-6}\ \mathrm{cm}^2/\mathrm{s}$$

where k_b is the Boltzmann constant, T = 310 K is the temperature, η is the viscosity of water at 37 °C, and a = 0.4 nm is the estimated radius of gyration of DAPI.

Nondimensionalization of the Diffusion Equation. For simulation simplicity, we used a dimensionless form of diffusion equation derived from the following steps:

$$\frac{\delta C}{\delta t} = D\nabla^2 C$$

where C is the concentration. The equation was nondimensionalized by inserting

https://doi.org/10.1021/acsbiomaterials.0c01365
ACS Biomater. Sci. Eng. XXXX, XXX, XXX−XXX

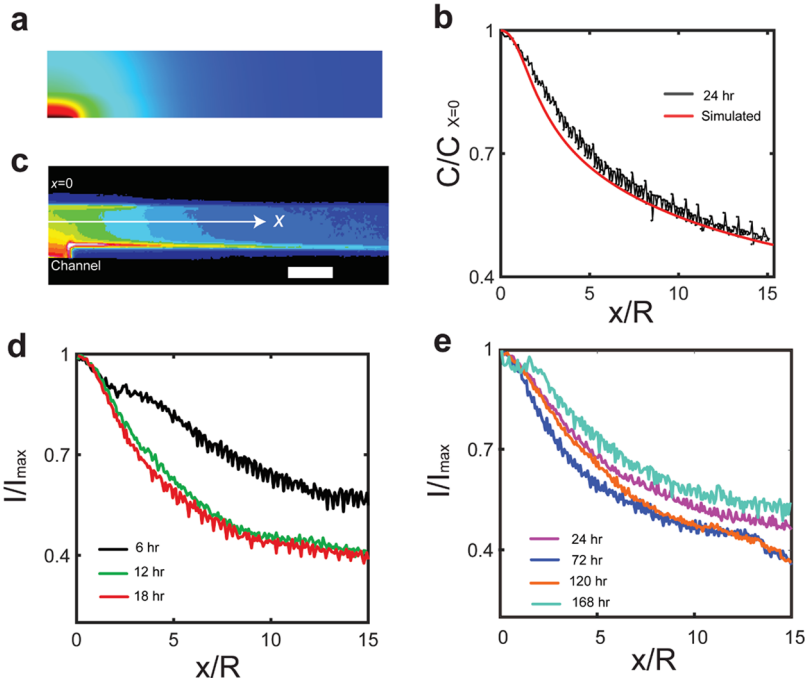

Figure 2. Simulation and calibration of gradient established in LPaD devices. (a) Simulated gradient profile at a simulation time equivalent to 24 h. (b) Simulated gradient profile (red) plotted with an average concentration profile measured at 24 h. (c) Confocal reconstructed side view of a DAPI infused hydrogel layer above the channel opening. DAPI intensity is highest at the center (red) and lowest on the side (blue); bulk DAPI concentration = 10 μg/mL; scale bar, 200 μm. Images were taken at t = 24 h. (d) Normalized intensity profiles from different time points plotted against normalized distance from the center of the channel along the x-direction; x = 0 at channel center as shown in panel a. Average normalized intensity profiles measured from n devices and m images at 6 h (n = 4, m = 8), 12 h (n = 4, m = 6), and 18 h (n = 5, m = 8). (e) Normalized intensity profiles from different time points plotted against normalized distance from the center of the channel along the x-direction; x = 0 at channel center as shown in panel a. Average normalized intensity profiles measured from n devices and m images at 24 h (n = 3, m = 6), 72 h (n = 5, m = 8), 120 h (n = 4, m = 7), and 168 h (n = 3, m = 4).

$$\tilde{C} = \frac{C}{C_0}$$

$$\tilde{t} = \frac{t}{\tau}$$

$$\tilde{\nabla} = \nabla L$$

where the characteristic length, L = 100 μm, is the typical channel radius. The equation then becomes

$$\frac{\delta \tilde{C}}{\delta \tilde{t}} = \frac{\tau}{L^2} \mathrm{D} \tilde{\nabla}^2 \tilde{C}$$

By setting $\frac{\tau}{L^2}\mathrm{D} = 1$ in the simulation, we get the following relationship:

$$\tau = \frac{L^2}{D} = 12 \text{ s}$$

which is the real-time equivalent of a simulation step. We used this value to calculate the necessary number of simulation steps for the simulation of different durations. For example, to simulate a real-time equivalent of 24 h, we need 7000 steps.

Simulation Setup and Boundary Conditions. We set the boundary conditions as indicated in Figure S3 to approximate our experimental condition; note that the channel width is the characteristic length that we used in nondimensionalization and, therefore, would always be 1 in the simulation. Since the diffusivity of molecules in hydrogel (D_H) is usually smaller than that in water (D_w), we simulated the hydrogel layer by adding a region with a smaller diffusivity. We found that, when we set D_H = 0.15, the simulated results best match our experimental results. At x = 40, we imposed a no flux boundary condition to simulate the channel confined by the inlet/outlet PDMS walls and the walls of the well plate. The initial condition is C = 0 everywhere except for at the channel, which is C = 1 at all times. Concentration is time-dependent except for at the channel and when far away from the channel (y = 75), where the concentration is always zero.

Microscopy and Image Analysis. An epifluorescence microscope (Leica, DMi8) was used to image stained cell samples. A confocal microscope (Nikon A1) was used to take x–y scans at different z locations for stained cell samples, as well as to characterize chemical gradients around the hydrogel slits. Images were processed and analyzed using ImageJ and NIS elements. To obtain concentration profiles, an image along the x–z plane of the slit was reconstructed, and fluorescent intensity was measured at the top of the gelatin layer.

Statistics. Statistical analysis was performed using GraphPad Prism. For statistical comparisons between two data sets, P-values were calculated using the student t-test function. For statistical comparisons between three or more data sets, P-values were calculated using one-way ANOVA with Tukey posthoc analysis.

RESULTS

Device Design and Fabrication. To induce a sustained chemical concentration gradient with a defined source location, we designed a two-layer LPaD device composed of a chemical reservoir and a thin PDMS film (thickness: 1/32 in.) with a slit of 200 μm in width generated by a laser cutter (Figure 1 and Figure S1). Target chemicals were loaded in the two chambers from the sides, which were connected to the chemical reservoir. To induce sustained passive diffusion, the slit in the PDMS film was filled with gelatin gel cross-linked *via* transglutaminase. In this way, the molecules loaded into the reservoir slowly diffused across the gelatin layer with tunable

https://doi.org/10.1021/acsbiomaterials.0c01365
ACS Biomater. Sci. Eng. XXXX, XXX, XXX−XXX

diffusive patterns defined by the geometry and location of the slit in the PDMS film. The detailed fabrication method is described in the Methods section. As shown in Figure 1b,c, the location of the source can be arbitrarily designed using a laser cutter, which will facilitate integration with other systems.

Characterization of the Chemical Gradients in LPaD Devices. We next sought to characterize the device by mapping concentration profiles and evaluating the kinetics and stability of the chemical gradient established in the device. COMSOL Multiphysics was used to simulate the gradient profile in 2D (see the Methods section for details). As shown in Figure 2a,b, a clear concentration gradient is established through the entire cell culture region at a simulation time equivalent to 24 h. Quantitatively, our simulation revealed that at $x = 0R$ the concentration reaches a maximum of $0.453C_b$, where C_b is the bulk concentration in the chemical chamber. Far away at $x = 15R$, the concentration decreased to $0.218C_b$, or $0.48C_{x=0R}$ as plotted in Figure 2b. We further studied the effect of the channel size on gradient formation. As shown in Figure S4, changing the width of the slit can significantly change the profile of the gradient. To compare our results with exiting microfluidic gradient generation devices, we calculated the specific gradient, which refers to a change in concentration over a cell distance divided by the average concentration over that distance,[28] for various designs. Our calculation showed that the specific gradient for the device shown in Figure 1 is 4.72×10^{-4} μm^{-1} and double the slit width will reduce the specific gradient to 4.02×10^{-4} μm^{-1}, while triple the slit width will further reduce the specific gradient to 3.66×10^{-4} μm^{-1}. Notably, while we used gelatin gels to seal the slit, changing the gel concentration did not significantly change the gradient profile (Figure S5). This is likely due to the small size of the slit compared to the size of the cell culture region.

To validate the simulation results, we used a small-molecule fluorescent dye DAPI as a probe as its molecular weight (277 g/mol) is close to those of many small molecules commonly used in stem cell differentiation. DAPI solution (bulk concentration = 10 μg/mL) was added to the chambers, and the cell culture chamber was filled with 1 × DPBS at 37 °C. To mimic the diffusivity of a confluent layer of cells and to visualize the concentration gradient, we cast a thin layer (<100 μm) of gelatin on the cell culture region only for the device calibration purpose. To acquire DAPI fluorescent intensities at different locations, we took confocal z-scans and reconstructed an averaged cross-section image along the $x-z$ plane from confocal stacks, where the slice thickness in the y-direction was around 100 μm. A typical cross-section ($x-z$ plane) colorimetric map of the fluorescent intensity profile is shown in Figure 2c. To quantify the intensity profiles, we measured the fluorescent intensity on the very top of the gelatin layer (along the white arrow in Figure 2c), although we observed a gradient throughout the entire depth of the gelatin layer. As shown in Figure 2b, the concentration immediately above the slit reaches the maximum and decreases to a plateau as it moves away from the slit, and the results were consistent with the COMSOL simulation. Our measurement in the $x-y$ plane also demonstrated that the gradient in the width direction of the cell culture region was shallow and steady across the whole device (Figure S6).

We next investigated the kinetics of the concentration profiles for a short time duration. We found that a gradient of DAPI fluorescence could be seen after 6 h of incubation, and by the 12th hour, the gradient profile was stabilized (Figure 2d). While a concentration gradient could be initiated immediately after adding DAPI, the gradient was not stable until 6 h after adding DAPI. A major challenge for patterning hPSCs using a chemical gradient is that the neural induction takes at least 168 h, and culture media need to be changed daily. Thus, we further investigated whether the chemical gradient can be reset and maintained at the previous level after media changes. To test this, on each day we washed and incubated the device in fresh 1 × DPBS for 1 h at the 23rd hour, followed by the addition of freshly prepared DAPI solution into the chemical chamber at the 24th hour. Using confocal microscopy, we found that the gradients could be maintained for at least 168 h, as shown in Figure 2e, as the concentration profiles did not change significantly with incubation time. To quantify the stability of the gradient, we divided the fluorescence intensity data into five sections along the x-axis and calculated the gradient in each section using the slope of linear fitting and performed one-way ANOVA analysis to test whether the gradient is stable over time (Figure S7). The results showed that, in most segments, the gradient was stable after 6 h, except for the first segment, where the gradient variation is significant. At section x/R = 12−15, a significant drop can be found at 120 and 72 h on the average intensity profile (Figure 2e). This variation is likely caused by smaller sample sizes for that section (Figure S7b). Nevertheless, no significant differences were found at region x/R = 12−15 from 12 to 72 and 168 h time points (Figure S7h). Together, our results validate that the chemical gradients can be quickly established within 12 h and can be robustly maintained for at least 7 days by resetting the device daily.

Response of MDCK Cells to CytoD. To test if cells can respond to the chemical gradients generated by the LPaD devices, we designed an assay leveraging the robust effect of CytoD on inhibiting actin polymerization in cells, which can be visualized by fluorescent dye conjugated phalloidin staining. In this experiment, we utilized a widely used epithelial cell line, Madin−Darby canine kidney (MDCK) cells, as our model system. Similar to neuroepithelial cells, MDCK cells form a highly packed monolayer once confluent and have been demonstrated to robustly respond to CytoD treatment.[29] MDCK cells were cultured on the LPaD device until confluent, and subsequently, 2.5 μM CytoD solution was added to the chemical chambers. After 24 h of incubation, the cells were fixed and stained with phalloidin and DAPI. When exposed to CytoD, the actin structures of MDCK cells appeared as punctuated dots, as indicated by yellow arrows in Figure 3a. We observed a significant amount of MDCK cells with depolymerized actin close to the slit, while almost all MDCK cells had intact actin cytoskeleton further away from the slit. To quantify the percentage of cells with actin puncta, the actin and DAPI staining images were first overlapped. The total cell number was determined using DAPI stained images by ImageJ. If puncta were found on any cell side, this cell was considered as a cell with depolymerized actin (Figure S8). As shown in Figure 3b, the percentage of cells with depolymerized actin decreased with increased distance from the slit, suggesting the existence of a CytoD gradient. Together, the results here demonstrate that cells cultured in LPaD devices can sense and respond to a chemical gradient established in the device. LPaD devices may potentially be utilized to study the collective migration and epithelial wound closure, using MDCK cells as an *in vitro* model system.

https://doi.org/10.1021/acsbiomaterials.0c01365
ACS Biomater. Sci. Eng. XXXX, XXX, XXX−XXX

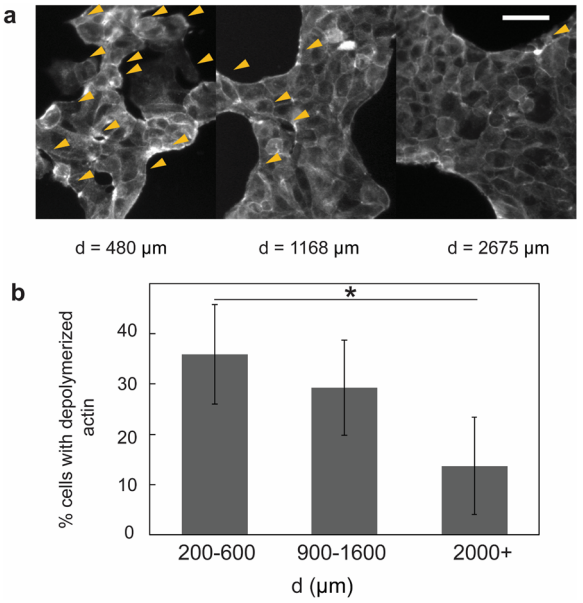

Figure 3. Cellular responses to a gradient of CytoD. (a) Typical fluorescence images of MDCK cells at different distances from the channel, fixed and actin stained with phalloidin; yellow arrows, depolymerized actin. Scale bar, 50 μm. (b) Percentage of depolymerized MDCK from exposure to 2.5 μM Cyto D for 24 h; n = 225, 223, and 245 for d = 200−600, 900−1600, and 2000+ μm, respectively. Data represent mean ± standard deviation from at least three independent experiments. *, $P < 0.05$.

Patterning Neuroepithelial Cell Sheet by Establishing a Shh Gradient. Next, we investigated whether hPSC-induced neuroepithelial cell sheets can be patterned dorsoventrally *via* a Shh gradient established in LPaD devices. In this experiment, LPaD devices with a slit on one side of the cell culture region were used (as shown in Figure 1c). We used dual SMAD inhibition and Wnt inhibition to induce hPSCs to forebrain fate.[30] Consistent with reported results, in this control condition, most of the cells express PAX6 by day 6 (Figure 4), indicating their dorsal anterior cell fate. It is well-established that Shh signal activation induces the ventralization of neuroepithelial cells.[31,32] Thus, we next tested whether a gradient of purmorphamine, a Shh agonist, can pattern the neuroepithelial cell sheet dorsoventrally. Purmorphamine solution (0.3 mL, 100 μM) was added to the chemical chamber, and differentiation media and purmorphamine solutions were changed daily until day 6 (the "Gradient" group in Figure 4). We found that, with the presence of a Shh gradient, cells grown close to the slit, where the purmorphamine concentration was high, showed a higher intensity of NKX2.1, a ventralizing transcription factor that depends on Shh signaling activation, while more cells expressed PAX6, a dorsal forebrain marker, away from the slit (Figure 4a, left panel). As a control, when purmorphamine (100 nM) was added to the cell culture region uniformly (the "Uniform Pur" group), NKX 2.1 intensity was higher than PAX6 uniformly across the entire region (Figure 4a, middle panel). When no purmorphamine was added (the "No Pur" group), a higher PAX6 intensity was found across the entire region (Figure 4a, right panel). We further quantified the percentage of PAX6 and NKX2.1 positive cells (see Figure S9 for methods) for different conditions (Figure 4b), and the results were consistent with the colorimetric maps. DAPI intensity quantification showed uniform cell densities across the cell culture region. We observed a significant decrease in the percentage of the NKX2.1 positive cells with increasing distance from the slit in the gradient group, while no statistically significant decrease was found in the control groups. It is important to seed hPSCs at an optimal density (75 000 cell/cm^2 in this case), as cell density can significantly affect the cell fate decision.[15,33] We found that, when the cells were seeded at a lower density (25 000 cells/cm^2), most cells were ventralized showing positive NKX2.1 staining (Figure S10).

DISCUSSION

In this work, we demonstrated a novel device, LPaD, that could generate a sustained chemical gradient for stem cell culture and differentiation. By modulating the geometry and location of the slit, the gradient profile can be precisely controlled. Most *in vitro* devices that claim to generate well-defined chemical gradients utilize microfluidic systems.[34−36] However, these systems were mainly used for short-term (∼hours) chemotaxis studies, and using these devices for long-term (∼weeks) stem cell culture applications is challenging. This is due to the difficulty in maintaining a strictly sterile environment and preventing the leakage and excessive evaporation of media. For stem cell differentiation experiments, the need to continuously provide fresh media and expensive morphogens for weeks makes it more difficult to use microfluidic systems for these applications. It was only recently that Bellan and colleagues reported a 3D hydrogel system with embedded channels to control morphogen delivery over extended periods of time and to pattern the differentiation of mesenchymal stem cells, but continuous pumping was still needed.[37] In contrast, our device design does not require tubing or wiring, can be placed into a conventional 6-well plate, and is autoclavable, greatly minimizing the risk of contamination and lowering the technical barriers for biologists to adapt to new systems. Compared to existing perfusion-based systems,[16] our device provides versatile control of the gradient profile, which is critical to pattern stem cells *in vitro*.

Another important aspect of gradient-generating devices is the stability of the gradients, especially in long-duration experiments. With time, the chemical source can be depleted and the low concentration region can be saturated, losing the gradients. While microfluidic-based devices use large circulating reservoirs to maintain the gradients, passive-diffusion-based devices can face the problem of diminishing gradients. To avoid this problem, we designed our devices such that both the chemical chamber and the outer cell culture media chamber can be easily refreshed. From our results, we can see that the gradients can be generated as soon as the sixth hour after introducing the chemical and stabilized at the 12th hour. If the chambers are refreshed every 24 h, the gradients can last for at least 168 h.

The recently developed 2D micropatterned culture systems are becoming powerful tools to model early stage human embryo development.[8−11] While most current works rely on spontaneous differentiation and a reaction−diffusion mechanism for self-patterning, there is a clear unmet need to integrate morphogen generation devices with those systems. For example, in the current *in vitro* gastrulation and ectoderm models, cell types from the trophectoderm and mesoendoderm layers are missing, respectively. Thus, their signals need to be represented by externally controlled chemical gradients. Very recently, Lutolf and colleagues designed an elegant microfluidic

https://doi.org/10.1021/acsbiomaterials.0c01365
ACS Biomater. Sci. Eng. XXXX, XXX, XXX−XXX

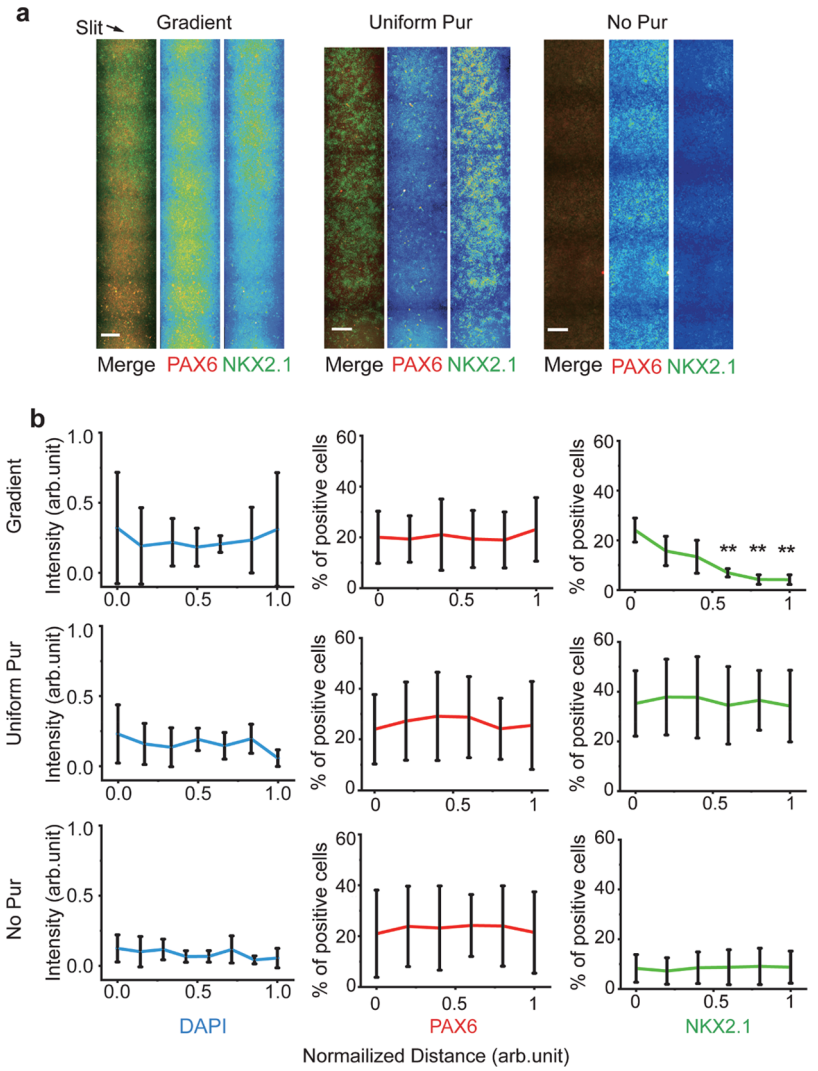

Figure 4. Gradient of Shh-agonist-induced dorsal−ventral patterning in hPSCs-derived neuroepithelial cell sheet. (a) hPSCs cultured on device in E6 medium with 100 nM LDN, 10 μM SB, and 5 μM XAV and the same medium with the addition of left, 100 μM purmorphamine in the chemical chamber (the "Gradient" group), n = 4; middle, 100 nM of purmorphamine homogeneously in the chemical chamber and cell culture chamber (the "Uniform Pur" group), n = 6; right, no purmorphamine homogeneously in the chemical chamber and cell culture chamber (the "No Pur" group), n = 5. Cells were fixed and stained on day 6 from the addition of purmorphamine. Red, PAX6; green, NKX2.1; scale bar, 200 μm. (b) Normalized fluorescence intensity of DAPI and percentage of PAX6 and NKX2.1 positive cells plotted against normalized distance to channel along the x-direction (length of the cell culture region) as indicated. Data represent mean ± standard deviation from three to five independent experiments. P-value was calculated by comparing with the first data point representing the intensity next to the slit. **, $P < 0.01$.

system to expose micropatterned hPSCs to localized morphogen sources and successfully demonstrated that such artificial signaling centers can induce symmetry breaking and germ layer patterning at the *gastrulation* stage.[15] Our work here further validated the concept that extrinsically modulated signaling centers can also effectively pattern embryonic tissues at the *neurulation* stage, highlighting the possibility to precisely engineer embryonic tissues *in vitro*. Future work should be done to integrate the LPaD device with the micropatterned neuroectoderm microtissue systems we developed and to generate a more precise *in vitro* neurulation model.[8,9]

The LPaD device has several limitations. Comparing to standard microfluidic device fabrication, the LPaD fabrication process does not require cleanroom access, which significantly lowers the adaptation barrier. However, it is more friendly to researchers with basic knowledge in laser cutting and soft lithography and still requires manual assembly, making it time-consuming to fabricate a large batch of devices. In our work, the concentration gradient was characterized using a fluorescent dye (DAPI). As the diffusivity of different morphogens varies depending on the molecular properties, it is necessary to empirically determine the initial concentration for optimal results. In addition, although we demonstrated that the slit dimension and the gel concentration can potentially change the gradient of morphogens, it is difficult to achieve a broad range of gradient steepness. Also, the LPaD device has a 2.5-fold gradient at a distance of 10 mm, while a large range of Shh concentrations (100−1000 ng/mL, 10-fold) have been used to derive cells with dorsal and ventral fates.[38] Thus, to expand the potential applications of the LPaD device, further modifications are needed to increase the range of gradient steepness.

Another potential caveat of the LPaD device is that the gradient is not stable for the first 6 h (Figure S7). Although a

https://doi.org/10.1021/acsbiomaterials.0c01365
ACS Biomater. Sci. Eng. XXXX, XXX, XXX−XXX

relatively short period of time, this early exposure to fluctuating levels of external signals may lead to unexpected effects on stem cell differentiation, making the stem cell differentiation results irreproducible. Numerous works, including our own, have demonstrated that the differentiation of hPSCs is very sensitive to temporal regulation of certain signaling pathways.[9,39] More specifically, Dessaud et al. demonstrated that the duration of Shh activation could control the dorsal−ventral patterning in neural tubes.[40] Thus, an important future direction is to improve the design to minimize the fluctuation of morphogen concentrations.

In conclusion, we have demonstrated a novel gradient-generating device design, where no tubing or pumps are necessary. The LPaD device can generate well-defined and complex concentration gradients in 2D, mimicking *in vivo* biochemical gradients during embryogenesis. With proper maintenance, the gradients can be sustained for up to 168 h. Using the LPaD device, we demonstrated that hPSCs-derived neuroepithelial cell sheets can be patterned dorsoventrally using an extrinsic Shh signaling source. We believe our LPaD device will be a powerful tool for organ-on-chip fabrication and studying human embryogenesis *in vitro*.

■ ASSOCIATED CONTENT

Supporting Information

The Supporting Information is available free of charge at https://pubs.acs.org/doi/10.1021/acsbiomaterials.0c01365.

Table of antibodies used in immunocytochemistry assays and figures of cell culture device and gradient measurement device schematics, acrylic LPaD device photo, boundary conditions for simulation schematic, simulated gradient profiles, cell culture area of a device used for stem cell experiments schematic, fluorescence images, normalized individual and average intensity profiles, linear fit of normalized intensity profiles, linear fit slope of normalized intensity data, images of stained MDCK cells, maging processing for quantifying the percentage of PAX6 and NKX2.1 positive cells, and immunofluorescence images (PDF)

■ AUTHOR INFORMATION

Corresponding Author

Yubing Sun − *Department of Mechanical and Industrial Engineering, Department of Biomedical Engineering, and Department of Chemical Engineering, University of Massachusetts Amherst, Amherst, Massachusetts 01003, United States;* orcid.org/0000-0002-6831-3383; Email: ybsun@umass.edu

Authors

Ningwei Li − *Department of Mechanical and Industrial Engineering, University of Massachusetts Amherst, Amherst, Massachusetts 01003, United States*

Feiyu Yang − *Department of Mechanical and Industrial Engineering, University of Massachusetts Amherst, Amherst, Massachusetts 01003, United States*

Subiksha Parthasarathy − *Department of Biomedical Engineering, University of Massachusetts Amherst, Amherst, Massachusetts 01003, United States*

Sarah St. Pierre − *Department of Mechanical and Industrial Engineering, University of Massachusetts Amherst, Amherst, Massachusetts 01003, United States*

Kelly Hong − *Amherst College, Amherst, Massachusetts 01003, United States*

Narciso Pavon − *Neuronscience and Behavior Graduate Program, University of Massachusetts Amherst, Amherst, Massachusetts 01003, United States*

ChangHui Pak − *Department of Biochemistry and Molecular Biology, University of Massachusetts Amherst, Amherst, Massachusetts 01003, United States*

Complete contact information is available at: https://pubs.acs.org/10.1021/acsbiomaterials.0c01365

Author Contributions

[▽]N.L. and F.Y. contributed equally to this work. N.L., F.Y., and Y.S. designed the experiments. N.L., F.Y., S.P., and K.H. fabricated the LPaD devices. N.L. and F.Y. performed device calibration and stem cell differentiation experiments. S.S. and F.Y. performed COMSOL simulations. N.L., F.Y., C.P., and Y.S. wrote the manuscript. All authors edited and approved the manuscript.

Notes

The authors declare no competing financial interest.

■ ACKNOWLEDGMENTS

This work was supported in part by the National Science Foundation (CMMI 1662835 and CMMI 1846866 to Y.S.), University of Massachusetts Amherst/Institute of Applied Life Sciences faculty start-up fund (C.P.), and the Initiative on Neurosciences Seed Grant at the University of Massachusetts Amherst (Y.S. and C.P.). This investigation was supported by National Research Service Award T32 GM135096 from the National Institutes of Health. The authors acknowledge the University of Massachusetts Amherst Light Microscopy Core for confocal microscopy services.

■ REFERENCES

(1) Hodge, R. D.; Bakken, T. E.; Miller, J. A.; Smith, K. A.; Barkan, E. R.; Graybuck, L. T.; Close, J. L.; Long, B.; Johansen, N.; Penn, O.; Yao, Z.; Eggermont, J.; Hollt, T.; Levi, B. P.; Shehata, S. I.; Aevermann, B.; Beller, A.; Bertagnolli, D.; Brouner, K.; Casper, T.; Cobbs, C.; Dalley, R.; Dee, N.; Ding, S. L.; Ellenbogen, R. G.; Fong, O.; Garren, E.; Goldy, J.; Gwinn, R. P.; Hirschstein, D.; Keene, C. D.; Keshk, M.; Ko, A. L.; Lathia, K.; Mahfouz, A.; Maltzer, Z.; McGraw, M.; Nguyen, T. N.; Nyhus, J.; Ojemann, J. G.; Oldre, A.; Parry, S.; Reynolds, S.; Rimorin, C.; Shapovalova, N. V.; Somasundaram, S.; Szafer, A.; Thomsen, E. R.; Tieu, M.; Quon, G.; Scheuermann, R. H.; Yuste, R.; Sunkin, S. M.; Lelieveldt, B.; Feng, D.; Ng, L.; Bernard, A.; Hawrylycz, M.; Phillips, J. W.; Tasic, B.; Zeng, H.; Jones, A. R.; Koch, C.; Lein, E. S. Conserved cell types with divergent features in human versus mouse cortex. *Nature* **2019**, *573* (7772), 61−68.

(2) Pollen, A. A.; Nowakowski, T. J.; Chen, J. D.; Retallack, H.; Sandoval-Espinosa, C.; Nicholas, C. R.; Shuga, J.; Liu, S. J.; Oldham, M. C.; Diaz, A.; Lim, D. A.; Leyrat, A. A.; West, J. A.; Kriegstein, A. R. Molecular Identity of Human Outer Radial Glia during Cortical Development. *Cell* **2015**, *163* (1), 55−67.

(3) Deglincerti, A.; Croft, G. F.; Pietila, L. N.; Zernicka-Goetz, M.; Siggia, E. D.; Brivanlou, A. H. Self-organization of the in vitro attached human embryo. *Nature* **2016**, *533* (7602), 251−4.

(4) Lancaster, M. A.; Renner, M.; Martin, C. A.; Wenzel, D.; Bicknell, L. S.; Hurles, M. E.; Homfray, T.; Penninger, J. M.; Jackson, A. P.; Knoblich, J. A. Cerebral organoids model human brain development and microcephaly. *Nature* **2013**, *501* (7467), 373−9.

(5) Qian, X. Y.; Song, H. J.; Ming, G. L. Brain organoids: advances, applications and challenges. *Development* **2019**, *146* (8), 166074.

(6) Quadrato, G.; Arlotta, P. Present and future of modeling human brain development in 3D organoids. *Curr. Opin. Cell Biol.* **2017**, *49*, 47−52.
(7) Sloan, S. A.; Andersen, J.; Paşca, A. M.; Birey, F.; Paşca, S. P. Generation and assembly of human brain region−specific three-dimensional cultures. *Nat. Protoc.* **2018**, *13* (9), 2062−2085.
(8) Xue, X.; Sun, Y.; Resto-Irizarry, A. M.; Yuan, Y.; Aw Yong, K. M.; Zheng, Y.; Weng, S.; Shao, Y.; Chai, Y.; Studer, L.; Fu, J. Mechanics-guided embryonic patterning of neuroectoderm tissue from human pluripotent stem cells. *Nat. Mater.* **2018**, *17*, 633−641.
(9) Xie, T.; Kang, J.; Pak, C.; Yuan, H.; Sun, Y. Temporal Modulations of NODAL, BMP, and WNT Signals Guide the Spatial Patterning in Self-Organized Human Ectoderm Tissues. *Matter* **2020**, *2* (6), 1621−1638.
(10) Haremaki, T.; Metzger, J. J.; Rito, T.; Ozair, M. Z.; Etoc, F.; Brivanlou, A. H. Self-organizing neuruloids model developmental aspects of Huntington's disease in the ectodermal compartment. *Nat. Biotechnol.* **2019**, *37* (10), 1198−1208.
(11) Knight, G. T.; Lundin, B. F.; Iyer, N.; Ashton, L. M. T.; Sethares, W. A.; Willett, R. M.; Ashton, R. S. Engineering induction of singular neural rosette emergence within hPSC-derived tissues. *eLife* **2018**, *7*, e37549.
(12) Dessaud, E.; McMahon, A. P.; Briscoe, J. Pattern formation in the vertebrate neural tube: a sonic hedgehog morphogen-regulated transcriptional network. *Development* **2008**, *135* (15), 2489−503.
(13) Wei, J.; Liu, C.; Jiang, Y.; Duan, C. Z.; Chen, L.; Li, W.; Liu, B.; Li, J. M. Microfluidic device for generating regionalized concentration gradients under a stable and uniform fluid microenvironment. *J. Micromech Microeng.* **2019**, *29* (1), 015008.
(14) Liu, W. M.; Han, K.; Sun, M. L.; Huang, Z. C.; Wang, J. Y. A Microfluidic Model with Hydrogel Barriers for the Construction of Shear-Free Attractive and Repulsive Cue Gradients. *Adv. Mater. Technol.* **2019**, *4* (2), 1800434.
(15) Manfrin, A.; Tabata, Y.; Paquet, E. R.; Vuaridel, A. R.; Rivest, F. R.; Naef, F.; Lutolf, M. P. Engineered signaling centers for the spatially controlled patterning of human pluripotent stem cells. *Nat. Methods* **2019**, *16* (7), 640.
(16) Tabata, Y.; Lutolf, M. P. Multiscale microenvironmental perturbation of pluripotent stem cell fate and self-organization. *Sci. Rep.* **2017**, *7*, 44711.
(17) Rahman, S. M.; Campbell, J. M.; Coates, R. N.; Render, K. M.; Byrne, C. E.; Martin, E. C.; Melvin, A. T. Evaluation of intercellular communication between breast cancer cells and adipose-derived stem cells via passive diffusion in a two-layer microfluidic device. *Lab Chip* **2020**, *20* (11), 2009−2019.
(18) Coluccio, M. L.; D'Attimo, M. A.; Cristiani, C. M.; Candeloro, P.; Parrotta, E.; Dattola, E.; Guzzi, F.; Cuda, G.; Lamanna, E.; Carbone, E.; Kruhne, U.; Di Fabrizio, E.; Perozziello, G. A Passive Microfluidic Device for Chemotaxis Studies. *Micromachines (Basel)* **2019**, *10* (8), 551.
(19) Sharei, A.; Zoldan, J.; Adamo, A.; Sim, W. Y.; Cho, N.; Jackson, E.; Mao, S.; Schneider, S.; Han, M. J.; Lytton-Jean, A.; Basto, P. A.; Jhunjhunwala, S.; Lee, J.; Heller, D. A.; Kang, J. W.; Hartoularos, G. C.; Kim, K. S.; Anderson, D. G.; Langer, R.; Jensen, K. F. A vector-free microfluidic platform for intracellular delivery. *Proc. Natl. Acad. Sci. U. S. A.* **2013**, *110* (6), 2082−7.
(20) Selimovic, S.; Sim, W. Y.; Kim, S. B.; Jang, Y. H.; Lee, W. G.; Khabiry, M.; Bae, H.; Jambovane, S.; Hong, J. W.; Khademhosseini, A. Generating nonlinear concentration gradients in microfluidic devices for cell studies. *Anal. Chem.* **2011**, *83* (6), 2020−8.
(21) Liang, D. Y.; Tentori, A. M.; Dimov, I. K.; Lee, L. P. Systematic characterization of degas-driven flow for poly(dimethylsiloxane) microfluidic devices. *Biomicrofluidics* **2011**, *5* (2), 024108.
(22) Mäki, A.-J.; Hemmilä, S.; Hirvonen, J.; Girish, N. N.; Kreutzer, J.; Hyttinen, J.; Kallio, P. Modeling and Experimental Characterization of Pressure Drop in Gravity-Driven Microfluidic Systems. *J. Fluids Eng.* **2014**, *137* (2), 021105.
(23) Demers, C. J.; Soundararajan, P.; Chennampally, P.; Cox, G. A.; Briscoe, J.; Collins, S. D.; Smith, R. L. Development-on-chip: in vitro neural tube patterning with a microfluidic device. *Development* **2016**, *143* (11), 1884−92.
(24) Cederquist, G. Y.; Asciolla, J. J.; Tchieu, J.; Walsh, R. M.; Cornacchia, D.; Resh, M. D.; Studer, L. Specification of positional identity in forebrain organoids. *Nat. Biotechnol.* **2019**, *37* (4), 436−444.
(25) Toepke, M. W.; Beebe, D. J. PDMS absorption of small molecules and consequences in microfluidic applications. *Lab Chip* **2006**, *6* (12), 1484−1486.
(26) Sasaki, H.; Onoe, H.; Osaki, T.; Kawano, R.; Takeuchi, S. Parylene-coating in PDMS microfluidic channels prevents the absorption of fluorescent dyes. *Sens. Actuators, B* **2010**, *150* (1), 478−482.
(27) Zheng, Y.; Xue, X.; Resto-Irizarry, A. M.; Li, Z.; Shao, Y.; Zheng, Y.; Zhao, G.; Fu, J. Dorsal-ventral patterned neural cyst from human pluripotent stem cells in a neurogenic niche. *Sci. Adv.* **2019**, *5* (12), No. eaax5933.
(28) Torisawa, Y. S.; Mosadegh, B.; Bersano-Begey, T.; Steele, J. M.; Luker, K. E.; Luker, G. D.; Takayama, S. Microfluidic platform for chemotaxis in gradients formed by CXCL12 source-sink cells. *Integr Biol. (Camb)* **2010**, *2* (11−12), 680−6.
(29) Cooper, J. A. Effects of cytochalasin and phalloidin on actin. *J. Cell Biol.* **1987**, *105* (4), 1473−8.
(30) Qi, Y.; Zhang, X. J.; Renier, N.; Wu, Z.; Atkin, T.; Sun, Z.; Ozair, M. Z.; Tchieu, J.; Zimmer, B.; Fattahi, F.; Ganat, Y.; Azevedo, R.; Zeltner, N.; Brivanlou, A. H.; Karayiorgou, M.; Gogos, J.; Tomishima, M.; Tessier-Lavigne, M.; Shi, S. H.; Studer, L. Combined small-molecule inhibition accelerates the derivation of functional cortical neurons from human pluripotent stem cells. *Nat. Biotechnol.* **2017**, *35* (2), 154−163.
(31) Elkabetz, Y.; Panagiotakos, G.; Al Shamy, G.; Socci, N. D.; Tabar, V.; Studer, L. Human ES cell-derived neural rosettes reveal a functionally distinct early neural stem cell stage. *Genes Dev.* **2008**, *22* (2), 152−165.
(32) Hu, B. Y.; Zhang, C. Differentiation of spinal motor neurons from pluripotent human stem cells. *Nat. Protoc.* **2009**, *4* (9), 1295−1304.
(33) Sun, Y.; Yong, K. M. A.; Villa-Diaz, L. G.; Zhang, X.; Chen, W.; Philson, R.; Weng, S.; Xu, H.; Krebsbach, P. H.; Fu, J. Hippo/YAP-mediated rigidity-dependent motor neuron differentiation of human pluripotent stem cells. *Nat. Mater.* **2014**, *13* (6), 599−604.
(34) Wang, X.; Liu, Z. M.; Pang, Y. Concentration gradient generation methods based on microfluidic systems. *RSC Adv.* **2017**, *7* (48), 29966−29984.
(35) Somaweera, H.; Ibraguimov, A.; Pappas, D. A review of chemical gradient systems for cell analysis. *Anal. Chim. Acta* **2016**, *907*, 7−17.
(36) Gupta, K.; Kim, D. H.; Ellison, D.; Smith, C.; Kundu, A.; Tuan, J.; Suh, K. Y.; Levchenko, A. Lab-on-a-chip devices as an emerging platform for stem cell biology. *Lab Chip* **2010**, *10* (16), 2019−2031.
(37) O'Grady, B.; Balikov, D. A.; Wang, J. X.; Neal, E. K.; Ou, Y. C.; Bardhan, R.; Lippmann, E. S.; Bellan, L. M. Spatiotemporal control and modeling of morphogen delivery to induce gradient patterning of stem cell differentiation using fluidic channels. *Biomater. Sci.* **2019**, *7* (4), 1358−1371.
(38) Liu, Y.; Weick, J. P.; Liu, H.; Krencik, R.; Zhang, X.; Ma, L.; Zhou, G. M.; Ayala, M.; Zhang, S. C. Medial ganglionic eminence-like cells derived from human embryonic stem cells correct learning and memory deficits. *Nat. Biotechnol.* **2013**, *31* (5), 440−7.
(39) Lian, X.; Hsiao, C.; Wilson, G.; Zhu, K.; Hazeltine, L. B.; Azarin, S. M.; Raval, K. K.; Zhang, J.; Kamp, T. J.; Palecek, S. P. Robust cardiomyocyte differentiation from human pluripotent stem cells via temporal modulation of canonical Wnt signaling. *Proc. Natl. Acad. Sci. U. S. A.* **2012**, *109* (27), E1848−57.
(40) Dessaud, E.; Yang, L. L.; Hill, K.; Cox, B.; Ulloa, F.; Ribeiro, A.; Mynett, A.; Novitch, B. G.; Briscoe, J. Interpretation of the sonic hedgehog morphogen gradient by a temporal adaptation mechanism. *Nature* **2007**, *450* (7170), 717−20.

https://doi.org/10.1021/acsbiomaterials.0c01365
ACS Biomater. Sci. Eng. XXXX, XXX, XXX−XXX